Electron-impact excitation of Li to high principal quantum numbers

M. Witthoeft, J. Colgan, and M. S. Pindzola
Department of Physics, Auburn University, Auburn, Alabama 36849, USA

C. P. Ballance and D. C. Griffin
Department of Physics, Rollins College, Winter Park, Florida 32789, USA

(Received 14 May 2003; published 27 August 2003)

The time-dependent close-coupling method is used to calculate electron-impact excitation cross sections for the $\mathrm{Li}(2s)\rightarrow\mathrm{Li}(n\ell)$ and $\mathrm{Li}(2p)\rightarrow\mathrm{Li}(n\ell)$ transitions at incident energies just above the ionization threshold. The implementation of the time-dependent close-coupling method on a nonuniform lattice allows the study of continuum-coupling effects in excitations to high principal quantum number, i.e., $n\leqslant 10$. Good agreement is found with *R*-matrix with pseudostates calculations, which also include continuum-coupling effects, for excitations to low principal quantum number, i.e., $n\leqslant 4$. Poor agreement is found with standard distorted-wave calculations for excitations to all principal quantum numbers, with differences still at the 50% level for $n=10$. We are able to give guidance as to the accuracy expected in the n^3 extrapolation of nonperturbative close-coupling calculations of low n cross sections and rate coefficients.

DOI: 10.1103/PhysRevA.68.022711 PACS number(s): 34.80.Kw

I. INTRODUCTION

Accurate electron-impact excitation cross sections and rate coefficients for atoms and their ions remain the key to collisional-radiative modeling of many astrophysical, atmospheric, and laboratory plasmas. For highly charged atomic ions, perturbative distorted-wave methods [1] may be used to treat both direct and resonant excitation processes. A recent example is the excellent agreement found between distorted-wave theory and electron-beam ion trap experiments for the $1s^2 2s\rightarrow 1s^2 3p$ transition in Fe^{23+} [2]. On the other hand, for neutral atoms and low charged atomic ions, the atomic levels may be strongly coupled so that nonperturbative methods, for example, *R*-matrix theory [3], are needed for accurate calculation of both direct and resonant excitation processes. Over the years, it has been found for many transitions that convergence of the excitation cross section is quite slow in regard to the number of atomic levels needed in the basis set eigenfunction expansion. Only with the recent development of nonperturbative methods that attempt to include a complete set of bound and continuum atomic levels has insight into the rate of convergence with the size of the basis set been provided. Recent examples include convergent close-coupling, *R*-matrix with pseudostates, and time-dependent close-coupling calculations for members of the Li isoelectronic sequence [4–7].

In this paper, the time-dependent close-coupling (TDCC) method is used to calculate electron-impact excitation cross sections for the $\mathrm{Li}(2s)\rightarrow\mathrm{Li}(n\ell)$ and $\mathrm{Li}(2p)\rightarrow\mathrm{Li}(n\ell)$ transitions at incident energies just above the ionization threshold. A nonuniform lattice [11] allows the study of continuum-coupling effects in excitations to high principal quantum numbers, i.e., $n\leqslant 10$. Comparisons are made with *R*-matrix with pseudostates (RMPS) calculations, which also include continuum-coupling effects, for excitations to low principal quantum number, i.e., $n\leqslant 4$. Comparisons are also made with non-pseudo-state *R*-matrix and distorted-wave calculations. We are able to give guidance to collisional-radiative modelers as to the accuracy expected in n^3 rule extrapolations of converged close-coupling and *R*-matrix with pseudostates calculations of low n cross sections and rate
coefficients.

The remainder of this paper is organized as follows. In Sec. II we give a brief description of the theoretical methods used to calculate electron-impact excitation cross sections for Li. In Sec. III we present electron-impact excitation cross sections for transitions from the ground and first excited states of Li at intermediate incident energies. Finally, in Sec. IV we summarize our findings. Unless otherwise stated, we use atomic units throughout this paper.

II. THEORY

The time-dependent close-coupling method has been discussed in detail for electron-hydrogen scattering [8,9] as well as electron-lithium scattering, where a pseudopotential is used to represent the inner shell electrons [10]. The TDCC method has recently been adapted for use on a variable spatial lattice and applied to electron-He^+ scattering [11]. An outline of the method follows.

The first step is to determine the set of bound and continuum orbitals supported on the variable lattice. The Hamiltonian for the valence electron is given by

$$h_\ell(r)=-\frac{1}{2}\frac{\partial^2}{\partial r^2}+\frac{\ell(\ell+1)}{2r^2}-\frac{Z}{r}+V_D(r)+V_x(r), \quad (1)$$

where $V_D(r)$ is the direct Hartree potential and $V_x(r)$ is a local exchange potential. The Hartree potential is calculated using a Li^+ $1s$ orbital generated in the Hartree-Fock approximation [12]. Additionally, the exchange potential contains a parameter that is adjusted to ensure agreement between the energy eigenvalues of this Hamiltonian and experimental measurements. Using a variable lattice, this Hamiltonian is nonsymmetric. The transformation [13]

$$T_{jk}=\sqrt{\frac{2}{h_j+\bar{h}_j}}\delta_{jk} \tag{2}$$

is applied to the Hamiltonian to obtain a symmetric form where h_j and $\bar{h}_j$ are the forward and backward lattice spacings, respectively, at r_j. The symmetric form of the Hamiltonian is diagonalized for each angular momentum ℓ to obtain energy eigenvalues and eigenvectors. The eigenvectors are transformed by applying T_{jk}^{-1} to recover the correct Li orbitals. In the frozen core approximation, the two $1s$ electrons in Li are stationary and are not involved directly in the scattering process. Therefore, we remove the $1s$ orbital generated by the diagonalization and make the $2s$ orbital effectively the ground state. This is done by removing the inner node of the $2s$ orbital using a pseudopotential. The other ns orbitals are then reconstructed to be orthogonal to the new $2s$ orbital. With the exception of the missing node, the new $2s$ orbital is very similar to the old $2s$ orbital. The removal of the inner node prevents any transition to the $1s$ state during time propagation.

To solve the scattering system, the total two-electron wave function is expanded in coupled spherical harmonics

$$\Psi^{LS}(\vec{r_1},\vec{r_2},t)=\sum_{\ell_1\ell_2}\frac{P^{LS}_{\ell_1\ell_2}(r_1,r_2,t)}{r_1r_2}\times\sum_{m_1m_2}C^{\ell_1\ell_2L}_{m_1m_20}Y_{\ell_1m_1}(\hat{r_1})Y_{\ell_2m_2}(\hat{r_2}), \tag{3}$$

where L and S are the total orbital and spin angular momentum of the system, $Y_{\ell m}(\hat{r})$ is a spherical harmonic, and $C^{\ell_1\ell_2\ell_3}_{m_1m_2m_3}$ is a Clebsch-Gordan coefficient. The time-dependent Schrödinger equation then takes the form

$$i\frac{\partial P^{LS}_{\ell_1\ell_2}(r_1,r_2,t)}{\partial t}=T_{\ell_1\ell_2}(r_1,r_2)P^{LS}_{\ell_1\ell_2}(r_1,r_2,t)+\sum_{\ell_1'\ell_2'}U^{L}_{\ell_1\ell_2,\ell_1'\ell_2'}(r_1,r_2)P^{LS}_{\ell_1'\ell_2'}(r_1,r_2,t), \tag{4}$$

where $T_{\ell_1\ell_2}(r_1,r_2)$ contains the kinetic energy, centrifugal barrier, nuclear, direct Hartree, and local exchange operators, and $U^{L}_{\ell_1\ell_2,\ell_1'\ell_2'}(r_1,r_2)$ couples the various $(\ell_1\ell_2)$ scattering channels.

The close-coupled partial differential equations are represented on a variable two-dimensional (2D) lattice using finite differencing methods. For excitation out of the $2s$ state, a (640×640)-point lattice is used, where the mesh spacing in each radial direction starts at 0.2 a.u. and is increased by 0.001 a.u. at each point until a maximum spacing of 0.5 a.u. is reached. With this spacing each radial direction spans 275 a.u. A smaller box size is used for excitation out of the $2p$ state; a (512×512)-point grid is used, which has a maximum size of 211 a.u.

The initial wave packet is an unsymmetric product function of the valence electron's orbital and an incoming Gaussian radial wave packet. This initial wave function is propagated in time using an explicit second-order differencing scheme. Collision probabilities can be calculated at any time by symmetrizing or antisymmetrizing the wave function according to the total spin of the system and projecting it onto products of the one-electron orbitals; for example, excitation probabilities are calculated using

$$\wp^{LS}_{n\ell}(t)=2\sum_{\ell'}\delta(\ell\ell'L)\times\left\{\int_0^\infty dr_2\left[\int_0^\infty dr_1P^{LS}_{\ell\ell'}(r_1,r_2,t)P_{n\ell}(r_1)\right]^2-\sum_{n'\ell'}\left[\int_0^\infty dr_2\int_0^\infty dr_1P^{LS}_{\ell\ell'}(r_1,r_2,t)\times P_{n\ell}(r_1)P_{n'\ell'}(r_2)\right]^2\right\}, \tag{5}$$

where $\delta(\ell_1\ell_2\ell_3)$ is a triangle identity and $P_{n\ell}(r)$ are the bound orbitals obtained by diagonalization of the one-electron Hamiltonian. The propagation continues for a time $t=T$ until the collision probabilities have converged to a constant value. After collision probabilities are calculated for a given total angular momentum L and spin S, excitation cross sections can be determined according to

$$\sigma(n\ell\rightarrow n'\ell')=\frac{\pi}{4k^2}\frac{1}{2\ell+1}\sum_L\sum_S(2L+1)(2S+1)\times\wp^{LS}_{n'\ell'}(t=T), \tag{6}$$

where $E=k^2/2$ is the incident electron energy. We performed TDCC calculations for both spin symmetries from $L=0$ to $L=7$.

Excitation cross sections may also be obtained using a standard distorted-wave method [14]. The first-order scattering amplitude is constructed using both direct and exchange Coulomb matrix elements. The bound radial orbitals are Hartree-Fock solutions [12], while the continuum radial orbitals are distorted by the field of a direct Hartree potential and a semiclassical local exchange potential. The perturbative distorted-wave method provides nonunitarized total cross sections for $\mathrm{Li}(2s)\rightarrow\mathrm{Li}(n\ell)$ and $\mathrm{Li}(2p)\rightarrow\mathrm{Li}(n\ell)$ transitions to arbitrary principal quantum number. As discussed in detail in the next section, we also use the standard distorted-wave method to provide a means of estimating partial cross sections from $L=8$ to $L=50$ for the time-dependent close-coupling calculations.

III. RESULTS

The TDCC and RMPS methods have been used before by Griffin *et al.* [7] to study electron-impact excitation for the $\mathrm{Li}(2s)\rightarrow\mathrm{Li}(n\ell)$ transitions with $n\leqslant4$. The results from

TDCC and 55-state RMPS calculations were compared to those from a 14-state *R*-matrix calculation without pseudostates, and a distorted-wave calculation. For that study, both the 55-state RMPS calculation and the 14-state *R*-matrix calculation were carried out for all partial waves up to $L=20$. However, for excitation out of excited states a partial-wave sum to $L=20$ is not sufficient. Therefore, in order to provide data for collisional radiative modeling in Li, we have extended our 55-state RMPS calculation to include all partial waves up to $L=60$. Since exchange is not important for the high partial waves, the partial cross sections from $L=10$ to $L=60$ were determined without exchange. Data for all transitions between the lowest nine terms of Li from these extended RMPS calculations are available at the Oak Ridge National Laboratory (ORNL) Controlled Fusion Atomic Data Center (CFADC) web site [15].

The previous TDCC results, calculated up to $L=10$, were supplemented by nine-state unitarized distorted-wave calculations in order to complete the summation. For transitions where there was good agreement between TDCC and the nine-state unitarized distorted-wave calculations at $L=10$ the unitarized distorted-wave results were used directly for $L>10$ up to $L=50$. There were some transitions where TDCC and unitarized distorted-wave calculations did not agree well at $L=10$. For those transitions, a cubic spline was used to match the TDCC results at $L=10$ to the unitarized distorted-wave results near $L=20$, where it was expected that the unitarized distorted-wave results should match the TDCC results well. After $L=20$, the unitarized distorted-wave results were then used to complete the summation to $L=50$.

For $n\leqslant 4$ excitations from the ground state of Li, the RMPS and TDCC results were in good agreement, but there were large differences between the results of these calculations and those from the 14-state *R*-matrix calculation. This illustrated the importance of including the continuum-coupling effects in scattering calculations, especially when the electron energy is near the ionization threshold.

As one would expect, standard distorted-wave and nine-state unitarized distorted-wave calculations also performed poorly for $n\leqslant 4$; however, it was unclear how their accuracy would change as n increased. The current calculations are made, in part, to resolve this issue by calculating excitation cross sections up to $n=10$. As a further study, cross sections are also calculated for excitation out of the $2p$ excited state of lithium. The new TDCC calculations are performed with incident electron energies of 10 eV and 15 eV for excitation out of the ground state and at 10 eV for excitation from the $2p$. The calculations went out to $L=7$ and the summation over L in Eq. (6) was completed in a similar manner as with the previous paper [7], except that the standard distorted-wave method was used instead of the unitarized distorted wave.

The difference between standard distorted-wave and unitarized distorted-wave methods depends on the specific transition under examination. In fact, the unitarized distorted-wave approach is closer to the 14-state *R*-matrix method than the standard distorted wave in terms of the calculation method and the results. Regardless, either distorted-wave method provides an effective way of completing the summation in Eq. (6), since they are very similar at large L. The key to matching the TDCC results at $L=7$ to the standard distorted-wave results near $L=20$ is understanding the behavior of the excitation cross sections at intermediate values of the total angular momentum ($L\approx 8$–20). To help us gain insight in this region, the results from the 55-state RMPS calculations are examined, not only from the ground state, but also from the $2p$ excited state. Below are two examples of how the RMPS results help guide the matching of the TDCC results at $L=7$ to distorted-wave results at $L=20$.

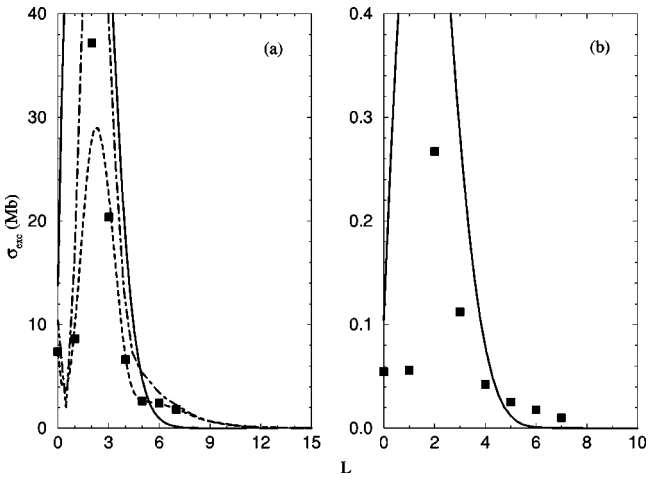

FIG. 1. Electron-impact excitation cross section for the (a) $\mathrm{Li}(2s)\rightarrow\mathrm{Li}(3s)$ and (b) $\mathrm{Li}(2s)\rightarrow\mathrm{Li}(10s)$ transitions at an incident electron energy of 10 eV. TDCC calculations are shown as filled squares, the dashed line is a 55-state RMPS calculations, the dot-dashed line is a 14-state *R*-matrix calculation, and the solid curve is a standard distorted-wave calculation.

We present in Fig. 1 the $2s\rightarrow 3s,10s$ transitions at an incident electron energy of 10 eV as an example of the difficulty that can arise in matching the TDCC results to the standard distorted-wave calculations. The TDCC points are shown as filled squares, the dashed and dot-dashed curves are spline fits to the 55-state RMPS and 14-state *R*-matrix calculations, respectively, and the solid curve is the distorted-wave result. If the TDCC calculations terminated at $L=5$, then one might guess that the TDCC calculations converge nicely to the distorted-wave result. Figure 1(a), however, shows that this is not the case. The TDCC points at $L=6,7$ show a flattening out of the excitation cross section, which is confirmed by the RMPS results. Figure 1(b), for the $2s\rightarrow 10s$ transition, shows that this behavior persists to large n. Although this feature does not contribute significantly to the total excitation cross section for this transition, it illustrates the need for caution when matching the TDCC results to the standard distorted-wave results.

Similar features are seen in the $2p\rightarrow 3p,10p$ transitions, which we show in Fig. 2. Again, for $L>5$, the TDCC results differ dramatically from the distorted-wave calculations. In this case, however, as indicated by the RMPS calculations shown in Fig. 2(a), the contribution to the total excitation cross section from intermediate L is much more significant

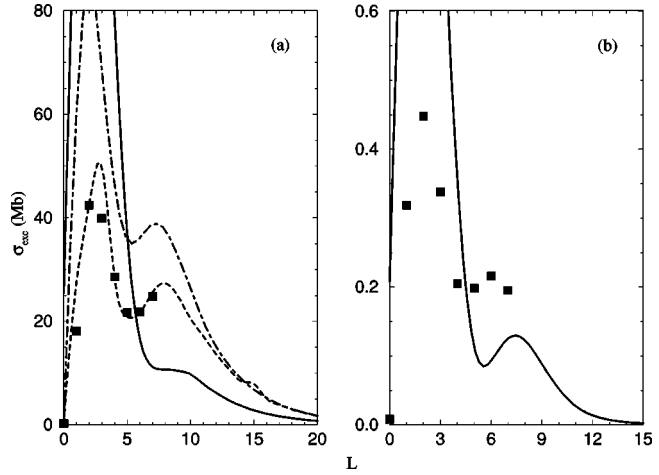

FIG. 2. Electron-impact excitation cross section for the (a) Li$(2p)\rightarrow$Li$(3p)$ and (b) Li$(2p)\rightarrow$Li$(10p)$ transitions at an incident electron energy of 10 eV. TDCC calculations are shown as filled squares, the dashed line is a 55-state RMPS calculations, the dot-dashed line is a 14-state *R*-matrix calculation, and the solid curve is a standard distorted-wave calculation.

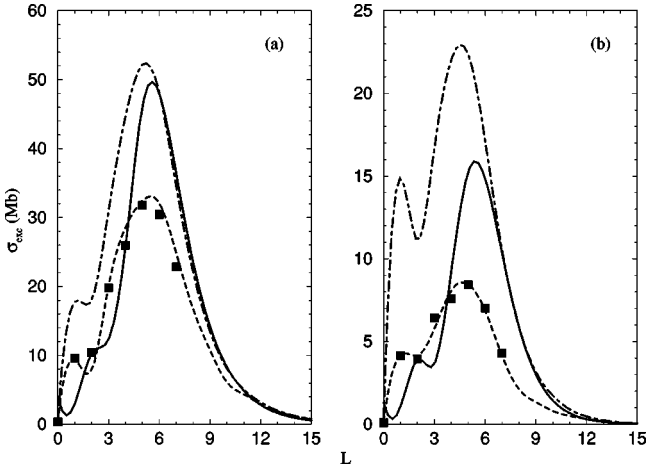

FIG. 3. Electron-impact excitation cross section for the (a) Li$(2s)\rightarrow$Li$(3d)$ and (b) Li$(2s)\rightarrow$Li$(4d)$ transitions at an incident electron energy of 10 eV. TDCC calculations are shown as filled squares, the dashed line is a 55-state RMPS calculations, the dot-dashed line is a 14-state *R*-matrix calculation, and the solid curve is a standard distorted-wave calculation.

than for the $2s\rightarrow 3s$ transition shown in Fig. 1(a). Disregarding the RMPS data in Fig. 2(a), it is easy to see the difficulty in correctly matching the TDCC data to the distorted-wave results for this transition. We point out that both Fig. 1 and Fig. 2 show monopole transitions, which have the worst agreement between TDCC and distorted-wave results at large L, whereas for most dipole transitions there is quite good agreement between TDCC and distorted-wave calculations at large L. For the actual matching of the TDCC data to the distorted-wave results, the RMPS results for $n=3,4$ are used as a guide to see how the nonperturbative results should behave at larger L. We then use this behavior to match the TDCC calculations to distorted-wave results for $n>5$ where no RMPS data exist.

The $2s\rightarrow 3d,4d$ and $2p\rightarrow 3d,4d$ transitions as a function of L are presented in Fig. 3 and Fig. 4. The first thing to note is how the TDCC and RMPS results converge toward both the standard distorted-wave and 14-state *R*-matrix results around $L=12$ for scattering out of the $2s$ state, and near $L=16$ for transitions from the $2p$. Thus, the current investigations of the behavior of the excitation cross sections at intermediate L clearly reveal that coupling effects between bound states and with the target continuum extend to quite large L. As can be seen in Fig. 4, the difference between the 14-state *R*-matrix calculation and the RMPS result is very significant in comparison to the total excitation cross section. By $L=20$, however, it appears that both the 14-state *R*-matrix and the standard distorted-wave calculations accurately represent the cross sections. Thus, the common practice of using a perturbative method such as plane-wave Born or distorted-wave calculations to determine the contributions from those higher partial waves that are below $L=20$ may be inaccurate for certain transitions in neutral systems. In fact, as our comparison with the 14-state *R*-matrix calculation reveals, the use of even a non-pseudo-state *R* matrix to provide the intermediate partial-wave contributions for an RMPS calculation can lead to error in the total cross section for neutral atoms. We have also investigated this for Be^+ and found that differences between RMPS and non-pseudo-state *R*-matrix calculations for a singly ionized species also persist to relatively high L, but the effects are much less significant.

Now that we have complete excitation cross sections for lithium out of both $n=2$ states, we can examine the trends that these cross sections exhibit as n increases. Several nonperturbative calculations such as convergent close coupling, RMPS, and TDCC, have revealed inaccuracies of well known perturbative methods in determining excitation and ionization cross sections for near-neutral systems. Since

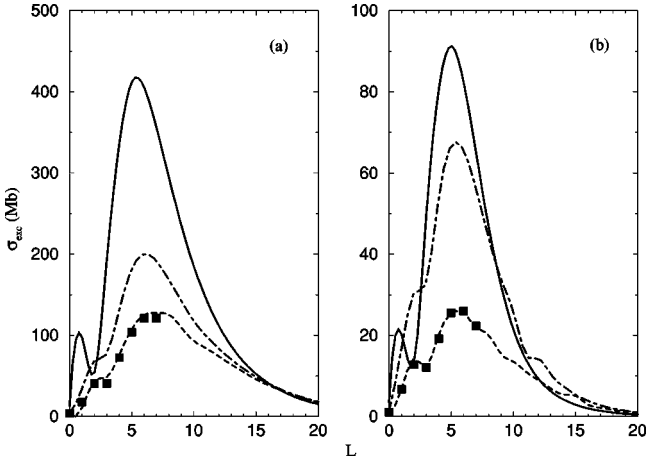

FIG. 4. Electron-impact excitation cross section for the (a) Li$(2p)\rightarrow$Li$(3d)$ and (b) Li$(2p)\rightarrow$Li$(4d)$ transitions at an incident electron energy of 10 eV. TDCC calculations are shown as filled squares, the dashed line is a 55-state RMPS calculations, the dot-dashed line is a 14-state *R*-matrix calculation, and the solid curve is a standard distorted-wave calculation.

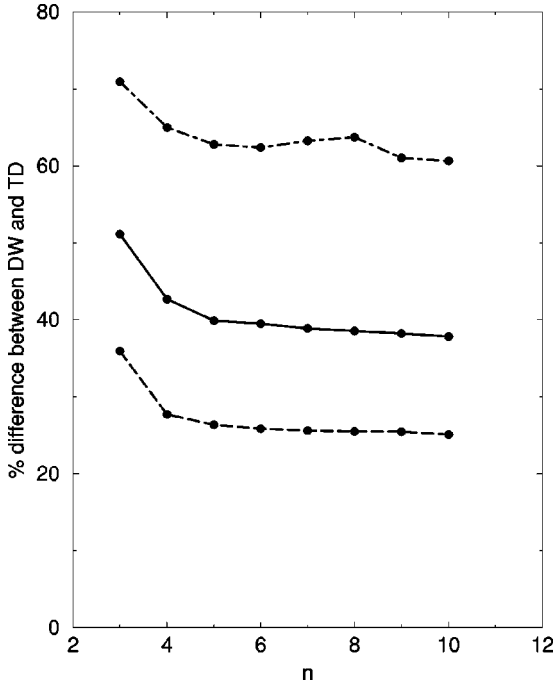

FIG. 5. Percentage difference between TDCC and standard distorted-wave excitation cross sections to the n manifold as a function of principal quantum number. Solid curve, 10 eV $2s \rightarrow n\ell$; dashed curve, 15 eV $2s \rightarrow n\ell$; dot-dashed curve, 10 eV $2p \rightarrow n\ell$.

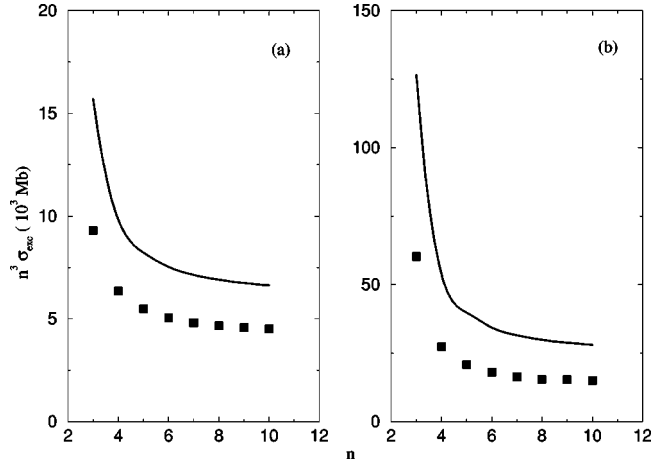

FIG. 6. n^3 scaling of excitation cross section versus principal quantum number at an electron incident energy of 10 eV for (a) $2s \rightarrow n\ell$ and (b) $2p \rightarrow n\ell$. The solid curve is from a standard distorted-wave calculation and the filled black squares are from TDCC calculations.

these nonperturbative calculations have typically been performed only for transitions up to $n=4$, it is unclear how the perturbative methods, such as the standard distorted-wave calculation, fare at large n. The current TDCC calculations using a variable lattice have extended the range in principal quantum number where excitation cross sections can be evaluated. We can now investigate how the accuracy of the standard distorted-wave calculations changes as n increases. In Fig. 5, we show the percentage difference between standard distorted-wave and TDCC excitation cross sections to the n manifold as a function of n. The solid curve and the dashed curve show the excitations from the $2s$ state at incident energies of 10 eV and 15 eV, respectively. The dot-dashed curve is excitation from the $2p$ state at 10 eV. For all curves, it is apparent that the accuracy of the standard distorted-wave calculations levels off as n increases, neither improving nor getting worse. The figure also indicates that the standard distorted-wave method becomes more accurate as the incident electron energy increases, but at the same energy is less accurate for excitations from the $2p$ excited state. Overall, it is interesting to see how poor the standard distorted-wave calculations are at low energies for the system in question, especially for excitations from the $2p$ level, where the standard distorted-wave calculations are almost a factor of 2 larger than the TDCC calculation. This difference is important for current plasma models where Li is used as a diagnostic [16].

The calculations to high n also allow us to investigate the validity of the n^3 scaling of the excitation cross sections. This scaling can be used to estimate cross sections to high n where few or no data exist. Figure 6 shows the scaling of both TDCC and standard distorted-wave calculations to $n=10$. The excitation cross sections plotted are to the n manifold; the solid curve is from the standard distorted-wave calculation, and the filled squares are the TDCC results. As can be seen in the figure, both the standard distorted-wave and TDCC calculations can be said to scale as n^3 for $n>6$. This should be important in plasma modeling calculations where accurate high n excitation cross sections could be obtained by properly scaling low n data. It would be best to have cross sections out to $n=6$ or $n=7$ for good results, but even $n=5$ results could be used to obtain more accurate cross sections than those from perturbative methods, such as distorted-wave calculations. If one is interested in determining the excitation cross sections to each particular configuration in n, including the quantum defect will improve the observed scaling. This will have the largest effect for scattering to the ns and np states.

IV. SUMMARY

We have performed time-dependent close-coupling calculations for scattering of electrons off neutral lithium in both the $2s$ ground state and the $2p$ excited state, using a variable lattice to obtain cross sections to high principal quantum number. These results were compared to those from an R-matrix with pseudostates calculation and a standard distorted-wave calculation. The RMPS results allowed us to study the behavior of the excitation cross sections at intermediate values of the total angular momentum ($L \approx 8-20$), which in turn allowed us to complete our TDCC calculations with greater confidence. Good agreement is found between the TDCC and RMPS results up to $n=4$, but the standard distorted-wave results disagree with both the RMPS and TDCC calculations at the 50% level. Comparison between

TDCC and the standard distorted-wave calculations up to $n = 10$ showed that both methods obey the expected n^3 scaling of the excitation cross section, but it was found that the distorted-wave approximation did not yield better cross sections as n increased; rather the percentage difference between distorted-wave and TDCC results was found to be relatively constant for larger n.

ACKNOWLEDGMENT

This work was supported in part by the U.S. Department of Energy. Computational work was carried out at the National Energy Research Scientific Computing Center in Oakland, CA, and at the Center for Computational Sciences in Oak Ridge, TN.

[1] N.F. Mott and H.S.W. Massey, *The Theory of Atomic Collisions* (Oxford University Press, London, 1965).
[2] M.S. Pindzola, Phys. Rev. A **65**, 014701 (2002).
[3] *Atomic and Molecular Processes*: *An R-Matrix Approach*, edited by P.G. Burke and K.A. Berrington (IOP Press, Bristol, 1993).
[4] K. Bartschat and I. Bray, J. Phys. B **30**, L109 (1997).
[5] P.J. Marchalant, K. Bartschat, and I. Bray, J. Phys. B **30**, L435 (1997).
[6] D.C. Griffin, N.R. Badnell, and M.S. Pindzola, J. Phys. B **33**, 1013 (2000).
[7] D.C. Griffin, D.M. Mitnik, J. Colgan, and M.S. Pindzola, Phys. Rev. A **64**, 032718 (2001).
[8] M.S. Pindzola and D.R. Schultz, Phys. Rev. A **53**, 1525 (1996).
[9] M.S. Pindzola and F. Robicheaux, Phys. Rev. A **54**, 2142 (1996).
[10] J. Colgan, M.S. Pindzola, D.M. Mitnik, and D.C. Griffin, Phys. Rev. A **63**, 062709 (2001).
[11] M.C. Witthoeft, M.S. Pindzola, and J. Colgan, Phys. Rev. A **67**, 032713 (2003).
[12] R.D. Cowan, *The Theory of Atomic Structure and Spectra* (University of California Press, Berkeley, CA, 1981).
[13] M.S. Pindzola, T.W. Gorczyca, and C. Bottcher, Phys. Rev. A **47**, 4982 (1993).
[14] M.S. Pindzola, D.C. Griffin, and C. Bottcher, in *Atomic Processes in Electron-Ion and Ion-Ion Collisions*, edited by F. Brouillard (Plenum Press, New York, 1986), p. 75.
[15] http://www-cfadc.phy.ornl.gov/data_and_codes
[16] W. Mandl, R. Wolf, M. von Hellermann, and H.P. Summer, Plasma Phys. Controlled Fusion **35**, 1371 (1993).